Modeling molecular mechanisms in the axon

R. de Rooij, K. E. Miller & E. Kuhl

Computational Mechanics
Solids, Fluids, Structures, Fluid-Structure Interactions, Biomechanics, Micromechanics, Multiscale Mechanics, Materials, Constitutive Modeling, Nonlinear Mechanics, Aerodynamics

ISSN 0178-7675
Volume 59
Number 3

Comput Mech (2017) 59:523-537
DOI 10.1007/s00466-016-1359-y

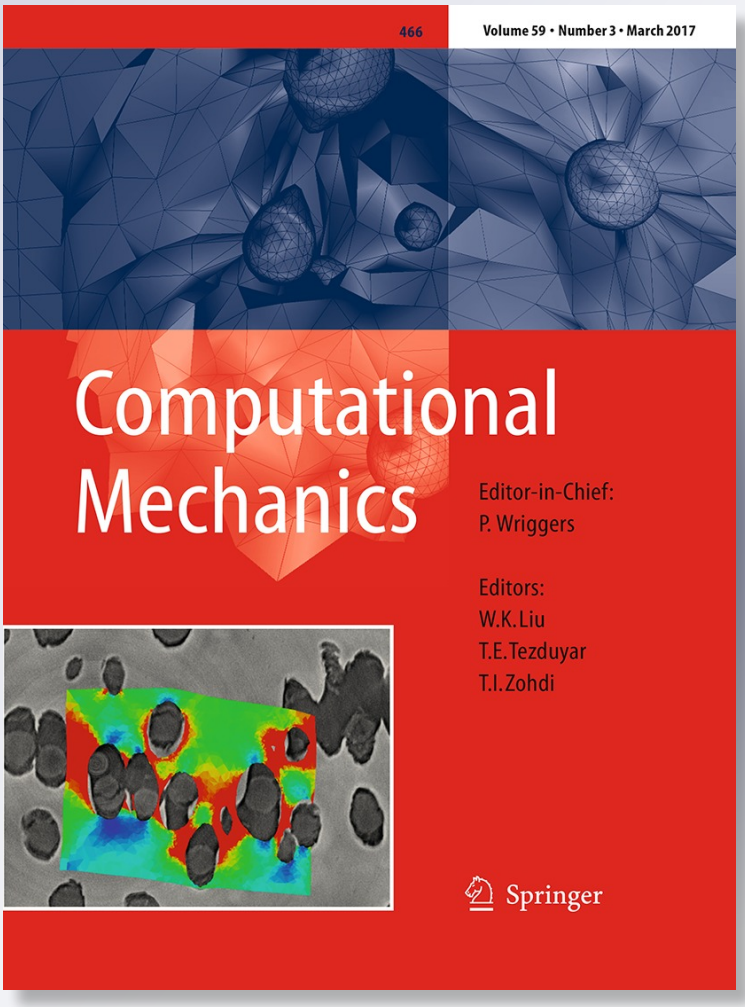

Springer

Comput Mech (2017) 59:523–537
DOI 10.1007/s00466-016-1359-y

ORIGINAL PAPER

Modeling molecular mechanisms in the axon

R. de Rooij[1] · **K. E. Miller**[2] · **E. Kuhl**[1]

Received: 5 September 2016 / Accepted: 8 November 2016 / Published online: 1 December 2016

Abstract Axons are living systems that display highly dynamic changes in stiffness, viscosity, and internal stress. However, the mechanistic origin of these phenomenological properties remains elusive. Here we establish a computational mechanics model that interprets cellular-level characteristics as emergent properties from molecular-level events. We create an axon model of discrete microtubules, which are connected to neighboring microtubules via discrete crosslinking mechanisms that obey a set of simple rules. We explore two types of mechanisms: passive and active crosslinking. Our passive and active simulations suggest that the stiffness and viscosity of the axon increase linearly with the crosslink density, and that both are highly sensitive to the crosslink detachment and reattachment times. Our model explains how active crosslinking with dynein motors generates internal stresses and actively drives axon elongation. We anticipate that our model will allow us to probe a wide variety of molecular phenomena—both in isolation and in interaction—to explore emergent cellular-level features under physiological and pathological conditions.

Keywords Finite element · Elasticity · Viscosity · Active force · Axon

✉ E. Kuhl
ekuhl@stanford.edu

[1] Departments of Mechanical Engineering and Bioengineering, Stanford University, Stanford, CA 94305, USA

[2] Department of Integrative Biology, Michigan State University, East Lansing, MI 48824, USA

1 Introduction

With a diameter of up to 14 μm and a length of up to 1m, the neuron is the largest cell in the human body, both in surface area and volume [42,57]. It is arguably also one of the most important cell types; it enables all communication with and within the brain through conducting electrical signals. The development of a neuron starts with the soma, the cell body, see Fig. 1. Several short dendrites extend from the soma into the surroundings, and *one* of these dendrites develops into the axon. In contrast to dendrites, the axon is long, it has a high degree of polarity alignment, and it is typically myelinated [21]. The axonal cytoskeleton consists of longitudinally aligned microtubules and neurofilaments that are connected by a variety of different crosslinks [20]. The cytoskeleton is encapsulated by an actin cortex [28,29] that is held together by spectrin [27,38,76]. At the tip of the axon, the growth cone is leading axonal growth and is responsible for path finding and axonal steering [48]. Extensive research has been devoted to neurons since their discovery in the 19th century with specific focus on axonal growth [20,33,48], the biophysics of axonal development [26,71], and the physiology of axons [23].

Throughout the past decade, several groups have recognized the importance of mechanical forces in the axon [7,25,71]. They found that the growth cone applies tension to the growing axon [11,12,46] and that it tightly regulates this tension within the physiological range of 1nN [24,40,60]. Numerous experiments have since been performed to quantify how these forces are transmitted along the axon. These experiments have established several generally accepted hypotheses that highlight the role of physical forces [34], for example during axonal development [8,33,71].

Single axon experiments in culture allow us to investigate the biophysics of individual molecules and molecular motors

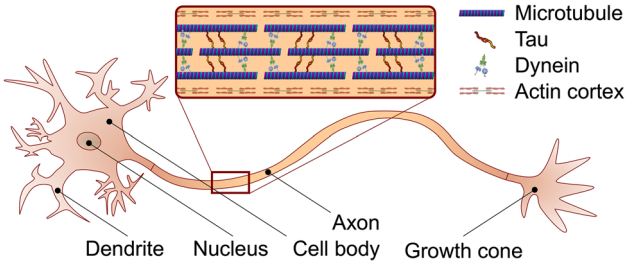

Fig. 1 Neuron and cross-sectional view of its axon. The development of a neuron starts with the cell body and several short dendrites. One of these dendrites develops into the axon, which is led by the growth cone. The axonal cytoskeleton is surrounded by an actin cortex and consists of longitudinally aligned microtubules that are connected by passive crosslinks such as tau and by active crosslinks such as dynein motors

within the axon. We now know that dynein is a unipolar molecular motor that generates axonal extensile forces by walking towards the minus end of microtubules [2,9,65]. Kinesin, likewise, is a bipolar molecular motor that walks towards the plus end of microtubules and causes microtubules to slide out of the neuronal cell body [18,49,77]. Myosin, in constrast, is a molecular motor that is located primarily in the actin cortex and in the growth cone where it generates contractile forces [14,53,80]. Force equilibrium and axonal elongation is a competition between the extensile forces of dynein and the compressive forces of myosin [29,33,65]. In addition to these actively force-generating motors, molecules like tau that passively crosslink the axonal cytoskeleton also play a critical role in network mechanics [81]. Although tau does not generate active forces, it stabilizes the axon by cross-linking neighboring microtubules and preventing them from depolymerizing. When exposed to strains or strain rates beyond the physiological limit, the tau-microtubule complex gradually weakens, which results in diffuse axonal injury and, ultimately, cell death [5,69,74].

Biological structures are living systems with the ability to adapt to their mechanical environment [61]. It is surprising that cells are often characterized as passive, time-independent, and purely elastic [64]. When constant forces are applied to an axon over a long period of time, it lengthens at a constant rate and displays a time-dependent behavior that is rheologically similar to a viscous fluid [44,54]. When constant forces are applied to the brain, for example during development or in response to tumor growth, the brain adapts gradually over time and displays a time-dependent behavior [35]. In response to body growth or artificial limb lengthening [83], axons can adapt and gradually grow in length [1,68,71]. Nonetheless, time-independent, elastic models have successfully been used to explain prestress in axons and in the brain [24] and to model the effects of high impact loading [4,58,74].

At present, the most popular approach is to model the adult nervous system as time-independent solid and the developing neuron as time-dependent fluid. Two more recent approaches suggest to interpret neurons as active fluids or solids [6,55,62] that are capable of generating active forces, conceptually similar to skeletal muscle [32,37]. In both cases, internal forces generated at the expenditure of adenosine triphosphate, ATP, explain internal tensions at the steady state as proposed by active matter hydrodynamics [51]. The active fluid model cleanly explains why axons elongate in response to large external forces, retract at low external forces, and maintain a constant rest length and rest tension at intermediate forces [55]. However, it does not consider the elastic behavior of the axon, which limits its use to sufficiently long time spans of observation. The active solid model [6,10] and the morphoelastic rod model [52] excellently capture the elastic properties of axons. The morphoelastic rod model characterizes the behavior of axons over long periods of time using the theory of finite growth [62]. It suggests that forces trigger the immediate addition of mass, whereas experiments indicate that forces first cause axons to stretch and then new mass is added gradually to restore the initial axonal diameter [39,47]. Further complicating this problem is the well-accepted observation that internal forces in cells change their viscoelastic properties: The measured mechanical properties of cells and tissues can be highly sensitive to the stresses and strains used to probe them [45,51,59]. This is especially important in growing neurons as it is recognized that molecular motors such as kinesin, dynein, and myosin generate forces that modulate axon elongation [3,41,49]. Taken together, this active nature of living systems makes it inherently difficult to measure, model, and understand neuronal mechanics. Given the complexity of this problem, the development of analytic equations and simulation tools that cleanly and simply model the problem of neuronal mechanics across all time scales and explain the complex dependence of effective elasticity and viscosity as a function of internal and external forces would be ideal.

The objective of this manuscript is to establish analytic equations and a finite element model that, for the first time, fully models the complex time and force dependent behavior of active and passive axonal substructures. We present a general framework to model a wide variety of molecular mechanisms within the an existing finite element infrastructure. Within this framework, we assign a user defined molecular mechanism to a standard finite element, whilst preserving the conceptual modularity of the finite element method. We demonstrate the potential of our method using a three-dimensional axon model that consists of microtubules and crosslinks. We examine two types of crosslinks, passive dissipative crosslinking and active motor crosslinking. We use these two mechanisms to interpret cellular-level characteristics such as axon stiffness, viscosity, and internal stress as emergent properties from the subcellular level. This allows us to inform constitutive models at the continuum level

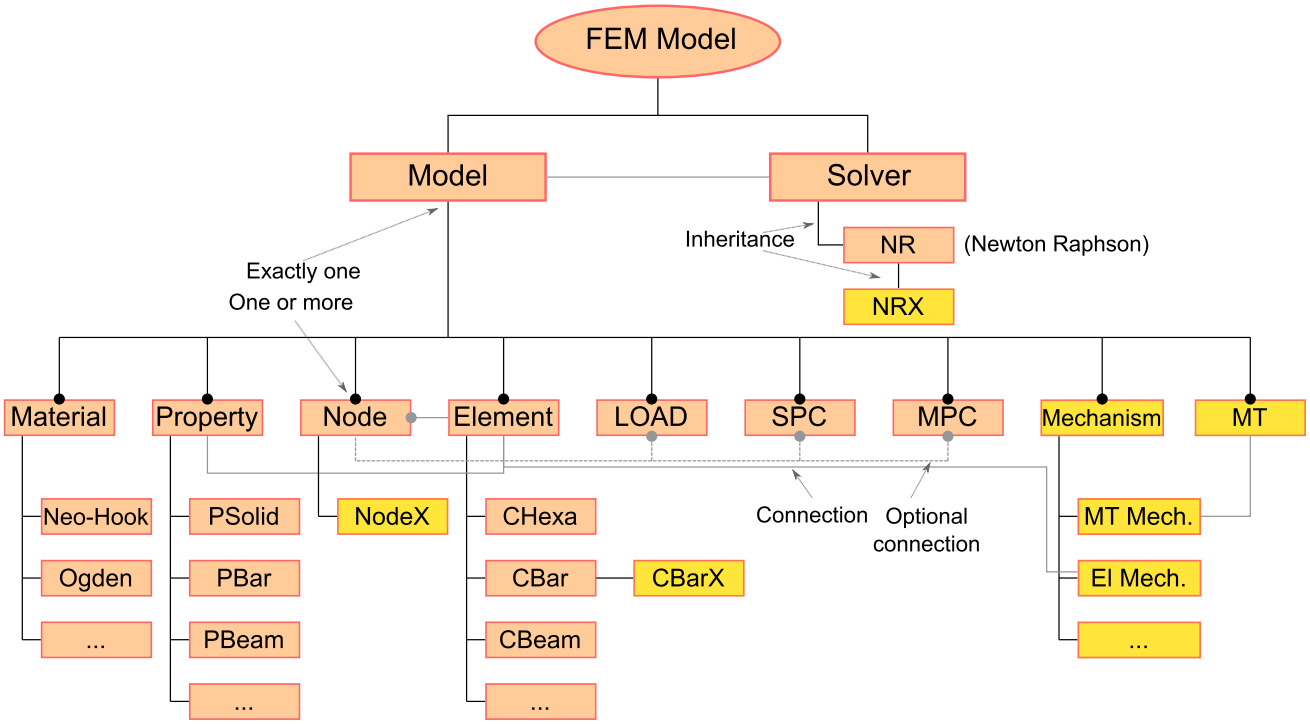

Fig. 2 General framework for modeling molecular mechanisms as an extension of the finite element method. *Orange boxes* represent objects that are available in a standard finite element infrastructure. *Yellow boxes* represent extensions to this general architecture that enable the modeling of molecular mechanisms. (Color figure online)

by molecular-level events. We then develop active viscoelastic fluid equations which we use to validate and understand the non-linear behaviors produced by the simulation. Importantly, this conceptual framework can be easily extended to all active systems including other types of cells and tissues.

The remainder of this manuscript is organized as follows: We begin by describing the general challenge of developing an algorithmic framework for dynamic mechanisms in living cells in Sect. 2. We describe the geometry and mechanical properties of our axon model in Sect. 3 and its basic mechanisms in Sect. 4. We then illustrate the key features of our model by means of two selected mechanisms in Sect. 5, and conclude by discussing our results in Sect. 6.

2 Algorithmic framework

Modeling molecular mechanisms within the context of the finite element method requires several extensions to the standard finite element infrastructure. Our main objective is to develop a generic and *modular* framework that will allow us to implement a wide range of molecular mechanisms. In practice, this implies that we only want to add to the existing finite element method—not change it—with the goal to plug in many different types of molecular mechanisms without affecting the overall algorithmic infrastructure. We provide an overview of the global implementation in Sect. 2.1 and discuss all extensions individually in Sects. 2.2–2.6.

2.1 Overview

Figure 2 illustrates the global architecture of our method. The orange boxes represent standard objects that are part of every standard implementation of the finite element method and the yellow boxes indicate the extensions that allow us to model a wide range of molecular mechanisms that are relevant for the axon.

The architecture consists of two main branches, the model and the solver. The first branch, the model, consists of the standard description of materials, properties, nodes, elements, point loads (LOAD), single point constraints (SPC), and multiple point constraints (MPC). Here we extend this structure with an extended node object (NodeX), an extended bar element (CBarX), mechanisms, and microtubule (MT) objects. The second branch, the solver, consists of at least an implementation of the Newton–Raphson method (NR) for nonlinear problems. Here we adopt the Newton–Raphson algorithm with slight modifications to allow for the application of molecular mechanisms. We implement this architecture into a custom-designed finite element framework.

Table 1 Parameter types and names of a standard Node object and an extended NodeX object

Node		NodeX	
`int`	`nid`	`int`	`nid`
`double`	`x,y,z`	`double`	`x,y,z`
`int[]`	`dofID`	`int[]`	`dofID`
		`Element`	`elMinus`
		`Element`	`elPlus`

Table 2 Parameter types and names of a standard CBar object and an extended CBarX object

CBar		CBarX	
`int`	`eid`	`int`	`eid`
`Node[]`	`nodes`	`NodeX[]`	`nodes`
`Property`	`prop`	`Property`	`prop`
		`double`	`restLength`
		`State`	`state`
		`NodeX[]`	`dummyNodes`
		`double`	`timeToNextEvent`
		`Mechanism`	`mechanism`

2.2 Node and NodeX objects

Table 1 compares the standard node and the extended node objects. A standard node (Node) is characterized by its nodal index, its coordinates, and the global indices of its degrees of freedom. An extended node (NodeX) also points to the elements on its plus and minus sides along the microtubule. This allows us to simulate molecular walking. When a molecule walks from one node on the microtubule to the next, it is essential for that node to know the elements on its plus and minus sides.

2.3 CBar and CBarX objects

Table 2 compares the standard bar element and the extended bar element. A standard bar element (CBar) is characterized by its element index, the two nodes it connects, and the element property. The extended bar element (CBarX) consists of several additional variables. The rest length of the element allows for active contraction or extension of the element. The current biological state of the element is a state variable that is important to identify the next action of an element. Table 3 summarizes potential element states. To keep track of the geometry, the extended bar element stores two dummy nodes to which the element was previously connected and may connect to again in the future. The variable `timeToNextEvent` monitors the time until this element has to perform its next event that is determined by the molecular `mechanism` that the element is subjected to.

Table 3 Possible states of a CBarX element

State	Description
`NoState`	Element has no state
`Microtubule`	Element is part of a microtubule
`CrosslinkAttached`	Crosslink that is attached to microtubules
`CrosslinkDetached`	Crosslink that is *not* attached to microtubules

Table 4 Parameter types and names of a Microtubule object

MT	
`int`	`n0,n1`
`int`	`e0,e1`
`MTstate`	`state`
`double`	`timeToNextEvent`
`MT`	`mtMinus`
`MT`	`mtPlus`
`Mechanism`	`mechanism`

Table 5 Examples of the parameter types and names of a Mechanism object, which vary for each mechanism and can be defined by the user

Mechanism for element		Mechanism for MT	
`double`	`tAttach`	`double`	`tPolym`
`double`	`tDetach`	`double`	`tDepolym`
		`double`	`tStationary`

2.4 Microtubule object

Table 4 summarizes the variables that constitute a microtubule object (MT). The microtubule object is specific to our extended architecture of the finite element implementation. A microtubule consists of many CBarX elements that collectively behave as a single microtubule. It consists of integer variables that contain the indices of the first and last nodes and elements that build up this microtubule. Similar to the CBarX elements, microtubules are characterized by their current state, the time to their next event, and the mechanism they are subjected to. Potential microtubule mechanisms could be polymerization and depolymerization. In addition the microtubule object has access to the microtubules at its minus and plus ends.

2.5 Mechanism object

Table 5 illustrates the type of variables of element-based and microtubule-based mechanisms. The mechanism object is our most important extension to the standard finite ele-

ment method as it allows us to simulate the dynamics induced by molecular mechanisms. The mechanism object is a super class and every individual mechanism is a sub class as highlighted in Fig. 2. Because of this general character, the common denominator among different mechanisms is not a set of variables, but simply the function `Apply()`. The `Apply()` function can be tailored to simulate the mechanism of molecular motors such as dynein, kinesin, or myosin, the detachment and reattachment of crosslinking proteins such as tau, or the polymerization and depolymerization of cytoskeletal filaments such as microtubules.

2.6 Solver

Algorithm 1 summarizes the pseudo code of our solver for a general solution step. The solver is based on a standard Newton–Raphson iteration with adaptive time-stepping, supplemented by modifications that allow for the execution of all mechanisms. The differences compared to a standard Newton–Raphson solver are the functions `UpdateModel()` and `RestoreModel()`. `UpdateModel()` is executed at the beginning of each step, and it applies all mechanisms for the duration of that particular step, see Algorithm 2. An action is performed if the `timeToNextEvent` variable of the CBarX element or MT object in Tables 2 or 4 becomes smaller than zero during the current step. `RestoreModel()` is only executed if the solver did not converge, in which case it restores the beginning of the step, see Algorithm 3.

Algorithms 2 and 3 only describe updating and restoring element-based mechanisms. The algorithms for updating and restoring microtubule-based mechanisms are conceptually similar, with the only difference that updating or restoring a microtubule also involves updating or restoring the elements that constitute that microtubule.

Algorithm 1 Pseudo code of modified Newton–Raphson solver with adaptive time stepping.

Step j
  Update model with `UpdateModel()`, see Algorithm 2.
  Solve system using iterative Newton–Raphson procedure, with `maxIter` as maximum number of iterations.
  if converged **then**
    Proceed to step $j+1$.
  else
    Restore model with `RestoreModel()`, see Algorithm 3.
    Decrease time step: $\Delta t \leftarrow \Delta t/2$.
    Repeat step j.
  end if
end

Algorithm 2 Pseudo code of `UpdateModel()` function.

UpdateModel()
  for all `Elements el` **do**
    Update time to the next event:
    `el.timeToNextEvent`$\leftarrow$`el.timeToNextEvent`$-\Delta t$.
    Apply mechanism: `el.mechanism.Apply()`.
    Note, before an element variable is updated by the mechanism, its old value is stored in `storage`. It can be restored by calling `RestoreModel()`, see Algorithm 3.
  end for
end

Algorithm 3 Pseudo code of `RestoreModel()` function.

RestoreModel()
  for `Element el` in `storage` **do**
    Restore stored variables of `el`.
    Restore time to next event:
    `el.timeToNextEvent`$\leftarrow$`el.timeToNextEvent`$+\Delta t$.
  end for
end

3 Axon model

In this section, we present the geometry and material properties of our axon model. Our axon consists of discrete microtubules, which are aligned along their longitudinal axis and connected by individual crosslinks. For now, we focus on modeling molecular mechanisms in the axonal cytoskeleton and neglect the axon cortex and the growth cone.

The first step in generating the geometry is to define the positions of the microtubules in a given cross section. Figure 3 illustrates 19 potential microtubule positions located on a triangular grid. On average, only half of these sites will be occupied in any given cross section. Each microtubule is connected to its neighbors by crosslinks which evolve dynamically as a result of different mechanisms.

The second step is to create the full three-dimensional axon model by extruding the cross section along the axon's long axis. Figure 4 shows a three-dimensional view of our axon model. At every potential microtubule site, we alternate between a microtubule of length l_{MT} and a void space of the same length l_{MT}. We distribute the microtubules randomly across the axon by starting with a random assignment of either microtubule or void at a random initial length. We discretize each microtubule with 2500 NodeX nodes and CBarX finite elements. We finalize the geometry by adding the crosslinks to the model. We randomly select one of the possible crosslinks in Fig. 3 at intervals of length Δx_{CL}. For the selected crosslink, we check whether microtubules are present at both of its ends. If so, we add the crosslink to the model using a CBarX finite element; if not, we proceed to the next interval. Motivated by electron micrographs of crosslinks in axons [38], we add all crosslinks at an angle of $\pm 10°$.

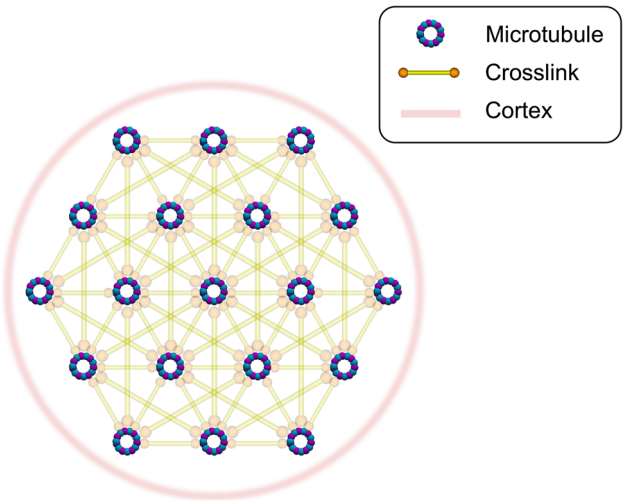

Fig. 3 Cross section of axon model. Each cross section consists of 19 potential microtubule locations with up to 12 crosslinks per microtubule. On average, only half of these locations are populated with microtubules [13,38]. Crosslinks between neighboring microtubules evolve dynamically as a result of different mechanisms

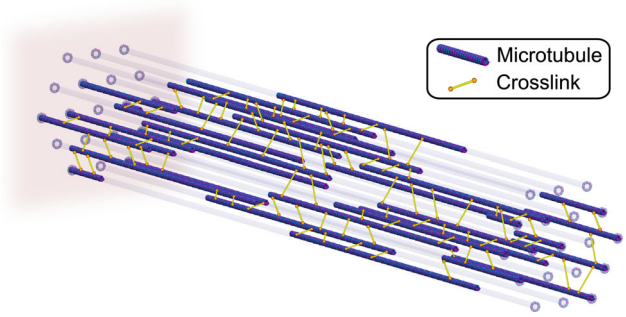

Fig. 4 Three-dimensional view of axon model. The axon is created by extruding the cross-section in Fig. 3 into the longitudinal direction. For visualization purposes, microtubule dimensions and crosslink density are not representative of the physiological parameterization

Figure 5 shows how we assign the `elMinus` and `elPlus` variables for each NodeX and the `n0`, `n1`, `e0`, `e1`, `mtMinus`, and `mtPlus` variables for each microtubule object. All microtubules are aligned with the minus end towards the cell body and the plus end towards the growth cone [79]. In addition to the nodes and elements that characterize the current state of the microtubules and crosslinks, two additional nodes, the `storageNodes`, are used as nodal connectivities of all detached crosslinks. We submerge the entire axon in a viscous fluid by connecting the first node of every microtubule to a fixed point on the left side of the axon using a viscous element. We set the viscosity of this surrounding fluid to $\eta = 10^{-7}$ MPa s, seven orders of magnitudes lower than our estimated axonal viscosity. This viscous fluid prevents numerical singularities in cases where a microtubule becomes fully disconnected from the remainder of the axon.

The boundary conditions of the axon include a clamp of the `storageNodes` and all nodes at the left end of the model representing the cell body. In addition, all nodes at the right end of the axon representing the growth cone are constrained to move together along the axonal direction using a MPC. For now, all nodes in the model are constrained to have no movement in the lateral direction. External forces can be applied anywhere along the axon, but are most commonly applied by the growth cone at the right end of the axon.

Table 6 Parameters of the axon model

Parameter	Value	Unit	References
Axon length	40	μm	[17]
Axon diameter	540	nm	
Microtubules per cross section	8.5	–	[13]
Microtubule length	10	μm	[78]
Microtubule stiffness	1200	MPa	[31]
Microtubule area	400	nm^2	[70]
Crosslink distance	1	nm	[38]
Crosslink angle wrt normal	10	deg	[38]
Crosslink stiffness	10	MPa	[50]
Crosslink area	1	nm^2	
Max. crosslink stretch	1.5	–	
External load	100	pN	[36,60,67]
Cytosol viscosity	10^{-7}	MPa s	

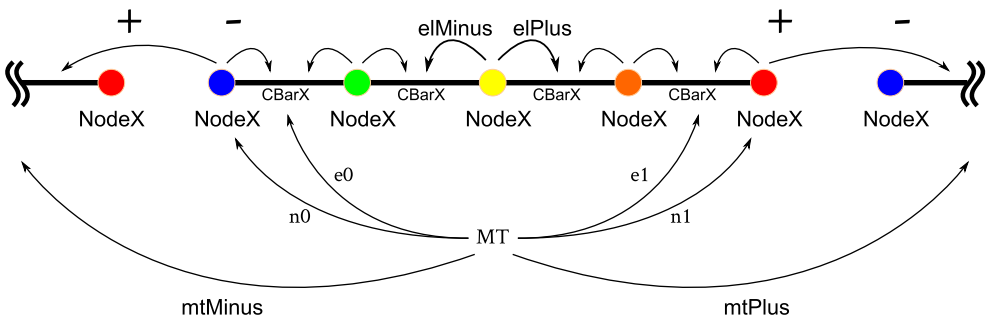

Fig. 5 A microtubule object consists of multiple nodes and elements. The *arrows* indicate the assignment of the `elMinus` and `elPlus` variables for each NodeX object with the minus end oriented towards the cell body, *left*, and the plus end towards the growth cone, *right*

Table 6 summarizes the geometric parameters and material properties for the microtubules and crosslinks. For simplicity, for now, we model all microtubules and crosslinks as linear elastic solids. This implies that all non-linearities and time-dependencies in the global axonal response emerge collectively from the mechanisms assigned to the crosslinks.

4 Molecular mechanisms

Our major focus is to explicitly model microscopic molecular mechanisms and to trace their macroscopic effects. To demonstrate our generic concept and the general implementation procedure, we highlight two different molecular mechanisms: passive dissipative crosslinking and active motor crosslinking. Before we turn to their implementation details, we illustrate the concept of molecular mechanisms by the simple mechanism of generic dynamic crosslinking, a detachment of a crosslink from its microtubules followed by a reattachment to the same nodes at some *randomly* chosen later time. To integrate this mechanism in our model, we first create a mechanism object, see Sect. 2.5, with two variables, `tAttach` and `tDetach`. We then assign this mechanism to the `mechanism` variable of each crosslink element, see Sect. 2.3, and, finally, we complete the `Apply()` function to enable the mechanism, see Sects. 2.5 and 2.6.

Algorithm 4 summarizes the pseudo code of the generic dynamic crosslinking mechanism. When the model is first initialized, every crosslink is *randomly* assigned to be either attached or detached from its microtubules, both with a 50% chance. The `Apply()` function then determines for each element whether an event has to be executed by checking the `el.timeToNextEvent` variable.

If the `el.timeToNextEvent` variable is negative and the crosslink is currently attached to microtubules, we change the nodal connectivity of this crosslink into the `storageNodes` of the model, see Sect. 3, which effectively detaches the crosslink. The nodes to which the crosslink used to be attached are stored in the `dummyNodes` variable of the element, the element `state` is updated to `CrosslinkDetached`, and a *randomly* chosen time between zero and `tAttach` is assigned to `el.timeToNextEvent`, which determines when the crosslink will reattach again.

If the `el.timeToNextEvent` variable is negative and the crosslink is currently detached, we change the nodal connectivity to the nodes stored in `dummyNodes`, which effectively reattaches the crosslink to the nodes it was previously attached to. We clear the variable `dummyNodes`, update `state` to `CrosslinkAttached`, and update `el.timeToNextEvent` to a *random* value between zero and `tDetach`. In both cases, we update the global element connectivity matrix of the model to account for changes in nodal connectivity.

Algorithm 4 Pseudo code of `mechanism.Apply()` function. The generic dynamic crosslinking mechanism defines crosslink detachment and reattachment to its original nodes. It is called for each element in each iteration of the modified Newton–Raphson solver, see Algorithms 1 and 2.

```
                                    ▷ Apply mechanism to Element el
if el.timeToNextEvent < 0 then
    Add element variables to storage.
    if el.state==CrosslinkAttached then
        el.dummyNodes←el.nodes
        el.nodes←storageNodes
        el.timeToNextEvent←random()*tAttach
        el.state←CrosslinkDetached
    else if el.state==CrosslinkDetached then
        el.nodes←dummyNodes
        el.dummyNodes←None
        el.timeToNextEvent←random()*tDetach
        el.state←CrosslinkAttached
    end if
    Update element connectivity matrix.
end if
```

4.1 Passive dissipative crosslinking

The mechanism of passive dissipative crosslinking involves the detachment of crosslinks from their from microtubules followed by a reattachment to different closeby nodes. Instead of reconnecting the crosslink back to its initial nodes, as described in Algorithm 4, the crosslink will now reconnect to nodes that are near by its initial nodes such that the crosslink length remains as close as possible to the rest length of the element. This mechanism is conceptually similar to generic dynamic crosslinking, but it additionally introduces the notion of viscosity at the global axon level.

On one end, one of the two nodes stored in `el.dummyNodes`, *randomly* picked with 50% chance, will reattach to the node that the crosslink detached from. On the other end, we search for the node that results in an optimal crosslink length. We start the search from the other node in `el.dummyNodes` and use the `elMinus` and `elPlus` of that node and its neighbors, see Sects. 2.2 and 3, to search in the plus and minus direction. We keep searching until we reach the node that yields the optimal crosslink length and attach the crosslink to this new node. This node is usually close to the node where we started the search and the node search can be efficiently completed in constant time per crosslink. This implies that the total computation time scales linearly with the total number of crosslinks and with the values of `tAttach` and `tDetach`. Figure 6 illustrates the mechanism of passive dissipative crosslinking.

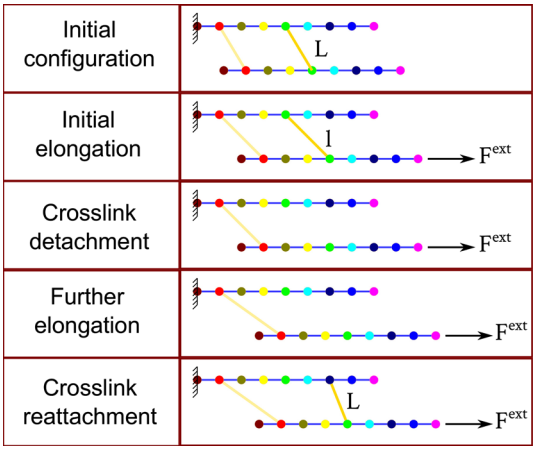

Fig. 6 Passive dissipative crosslinking. The mechanism of passive dissipative crosslinking involves elongation, detachment, elongation, and reattachment. By reattaching to a new nearby node, the crosslink dissipates energy as it restores its initial length

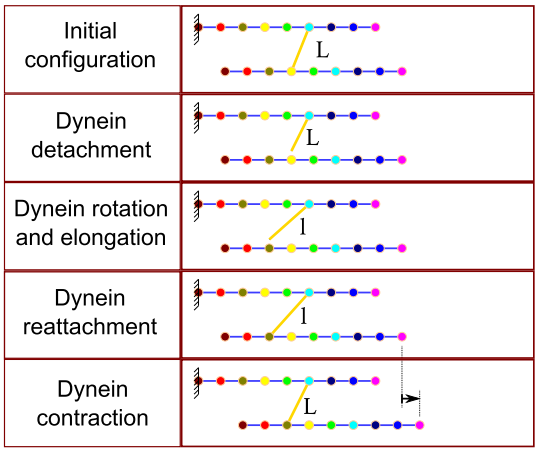

Fig. 7 Active motor crosslinking. The mechanism of active motor crosslinking involves detachment, elongation, reattachment, and contraction. By contracting back to its initial length, the dynein motor induces an active force

4.2 Active motor crosslinking

The mechanism of active motor crosslinking involves the detachment, elongation, reattachment, and contraction of dynein crosslinks. Instead of reconnecting the crosslink back to its initial nodes, as described in Algorithm 4, the dynein motor will remain attached at one end and reconnect at the other end to a further away node to elongate in length. Upon reattachment, active contraction will bring dynein back to its initial rest length. This mechanism is conceptually similar to the generic dynamic crosslinking, but it additionally introduces the notion of active force generation at the global axon level.

Cytoplasmic dynein consist of two heavy chains that are connected to each other on one end, and are both individually connected to a microtubule on the other end. On one end, dynein functions as a carrier for cargo, in our case, an individual microtubule [2]. Since the binding between dynein and the cargo microtubule is strong, we model this connection as fixed. On the other end, the dynein molecule walks towards the minus side of the highway microtubule by a repeating process of detachment and reattachment. The mechanism of these unipolar dynein molecules has been well characterized [43,66,73] and supported by experimental data [16,30,50,72].

Starting from the initial state, binding of adenosine triphosphate, ATP, at the walking domain of dynein detaches the dynein crosslink from the microtubule. The dynein chain then rotates towards the minus side of the microtubule and *extends*. Next, adenosine triphosphate hydrolysis leads to release of adenosine diphosphate (ADP) and, thereby, to a reattachment of the dynein motor to the microtubule. The final step is the powerstroke of dynein which *contracts* the molecule back to its initial length.

We model the mechanism of active motor crosslinking conceptually similar to the passive dissipative crosslinking mechanism in Sect. 4.1. The only difference is that now, only the second node of the crosslink, which represents the dynein walking domain, will reattach to a different node and the search for this new node is further away from the initial node, in the minus direction of the microtubule. We control the active contraction and extension by changing the element variable `el.restLength`, see Sect. 2.3, and we adopt an active contraction of $\lambda^{act} = L/l = 0.9$. Figure 7 illustrates the mechanism of active motor crosslinking.

5 Results

In this section, we explore how individual molecular-level events affect the cellular-level response. To homogenize the constitutive behavior of the axon, from the molecular to the cellular scale, we represent the axon using a viscoelastic Maxwell model with internal stress,

$$\dot{\varepsilon} = \frac{\sigma^{ext} + \sigma^{int}}{\eta} + \frac{\dot{\sigma}^{ext} + \dot{\sigma}^{int}}{E} \qquad \text{with } \eta = \tau\, E\,, \tag{1}$$

in which σ^{ext} and σ^{int} are the external and internal stresses, E is the elastic stiffness, and η is the coefficient of viscosity, which is related to the elastic stiffness via the relaxation time τ. External stresses arise from externally applied forces, whereas internal stresses are caused by forces that are generated inside the axon, e.g., forces applied by the powerstroke of dynein motors. We consider a creep test in which we apply a sudden external and internal stress and measure the macroscopic stress and strain at time Δt. We introduce the discrete time derivatives $\dot{\varepsilon} = \Delta\varepsilon/\Delta t = \varepsilon/\Delta t$ and

$\dot{\sigma} = \Delta\sigma/\Delta t = \sigma/\Delta t$, and obtain the following relation for the elastic stiffness E,

$$E = \left[1 + \frac{\Delta t}{\tau}\right] \frac{\sigma^{\text{ext}} + \sigma^{\text{int}}}{\varepsilon} . \tag{2}$$

We further introduce the effective or measured stiffness $E_{\text{eff}} = \sigma^{\text{ext}}/\varepsilon$ as the ratio of the externally applied stress σ^{ext} and the measured strain ε, and interpret the actual stiffness E as the effective stiffness E^{eff} scaled by the effects of viscoelasticity and internal stress,

$$E = \left[1 + \frac{\Delta t}{\tau}\right] \left[1 + \frac{\sigma^{\text{int}}}{\sigma^{\text{ext}}}\right] E^{\text{eff}} \quad \text{with } E^{\text{eff}} = \frac{\sigma^{\text{ext}}}{\varepsilon} . \tag{3}$$

Similar to the effective stiffness E^{eff}, we introduce the effective viscosity $\eta^{\text{eff}} = \sigma^{\text{ext}}/\dot{\varepsilon}$ as the ratio of the externally applied stress σ^{ext} and the strain rate $\dot{\varepsilon}$, and interpret the actual viscosity η as the effective viscosity η^{eff} scaled by the effects of internal stress,

$$\eta = \left[1 + \frac{\sigma^{\text{int}}}{\sigma^{\text{ext}}}\right] \eta^{\text{eff}} \quad \text{with } \eta^{\text{eff}} = \frac{\sigma^{\text{ext}}}{\dot{\varepsilon}} . \tag{4}$$

In the following two examples, we investigate how the molecular mechanisms of passive dissipative crosslinking and active motor crosslinking effect the overall axonal viscosity through the term $1 + \Delta t/\tau$ and the internal stress through the term $1 + \sigma^{\text{int}}/\sigma^{\text{ext}}$.

5.1 Passive dissipative crosslinking

To explore the effects of the molecular mechanism of passive dissipative crosslinking on whole axon rheology, we use the axon model from Sect. 3 and assign the dissipative dynamic mechanism of Sect. 4.1 to all crosslinks. On the molecular level, the crosslinks are stretched when they detach and unstretched when they reattach, which inherently induces energy dissipation. On the axon level, this behavior collectively manifests itself as viscosity, and the axon as a whole behaves as a rheological Maxwell element.

We perform a series of creep tests and apply an external force to the tip of the axon. We increase the external force to $F^{\text{ext}} = 100\,\text{pN}$ in the first time step and maintain this force during the remainder of the simulation. Unless stated otherwise, we use equal detachment and reattachment times of $\texttt{tDetach} = \texttt{tAttach} = 180\,\text{s}$ to maintain a constant average crosslink density. Our total simulation time is 2000 s and we use a time step of 10 s.

Figure 8 illustrates the typical simulation results of our model with passive dissipative crosslinking. The three discretizations show the axon at three consecutive time points of the simulation, top. The corresponding kymographs highlight

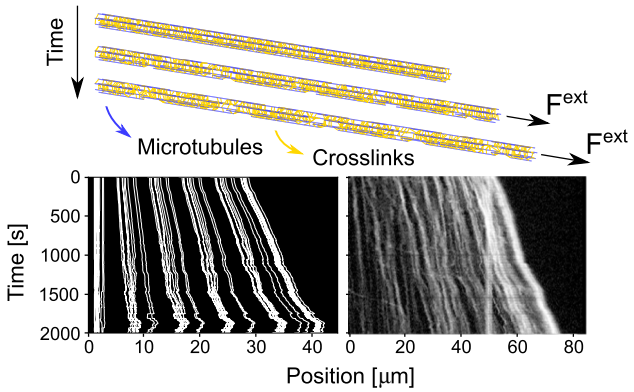

Fig. 8 Axon with dissipative dynamic mechanism assigned to each crosslink and loaded by an external tip force. The finite element discretization (*top*) shows the axon three consecutive time points. The corresponding numerical kymograph (*bottom left*) shows good qualitative agreement with the experimentally obtained kymograph (*bottom right*) [55]

the longitudinal position of all microtubules as a function of time, right. The computationally predicted kymograph, bottom left, shows an excellent qualitative resemblance with the experimentally measured kymograph [55], bottom right.

Figure 9 summarizes the typical readouts for a single simulation. The kymograph, top left, highlights the configuration of individual microtubules. For equal detachment and reattachment times $\texttt{tDetach}$ and $\texttt{tAttach}$, the number of crosslinks remains constant during the simulation, bottom left. The total stretch λ is composed of an initial elastic stretch, caused by the external force, followed by a linearly increasing viscous stretch, caused by the viscous crosslinking mechanism, top right. The linearly increasing stretch λ results in a constant stretch rate $\dot{\lambda}$, which we compute using a linear regression of the stretch over an interval of 200 s around t, middle right. The resulting macroscopic viscosity $\eta^{\text{eff}} = \sigma/\dot{\varepsilon}$, which we have calculated using Eq. (1) with the small strain assumption $\varepsilon = \lambda - 1$, increases initially but then remains constant, bottom right.

To explore the effects of our model parameters on macroscopic properties, we extract a single value for the axonal stiffness E and viscosity η from Fig. 9. We calculate the axon stiffness $E = \sigma^{\text{ext}}/\varepsilon$ using Eq. (3) for the stiffness of the first time step in which the total external force is applied. We define the external stress as $\sigma^{\text{ext}} = F^{\text{ext}}/A^{\text{axn}}$ with an axonal cross section area of $A^{\text{axn}} = \pi(r^{\text{axn}})^2$ and an axonal radius of $r^{\text{axn}} = 270\,\text{nm}$, see Table 6. We calculate the axon viscosity $\eta = \sigma^{\text{ext}}/\dot{\varepsilon}$ using Eq. (4) and average the viscosity across the time window of 400 and 2000 s to ensure that the model is in a steady state. Our model consists of several parameters that may effect the macroscopic axon properties. For brevity and to maintain focus, here we only investigate the

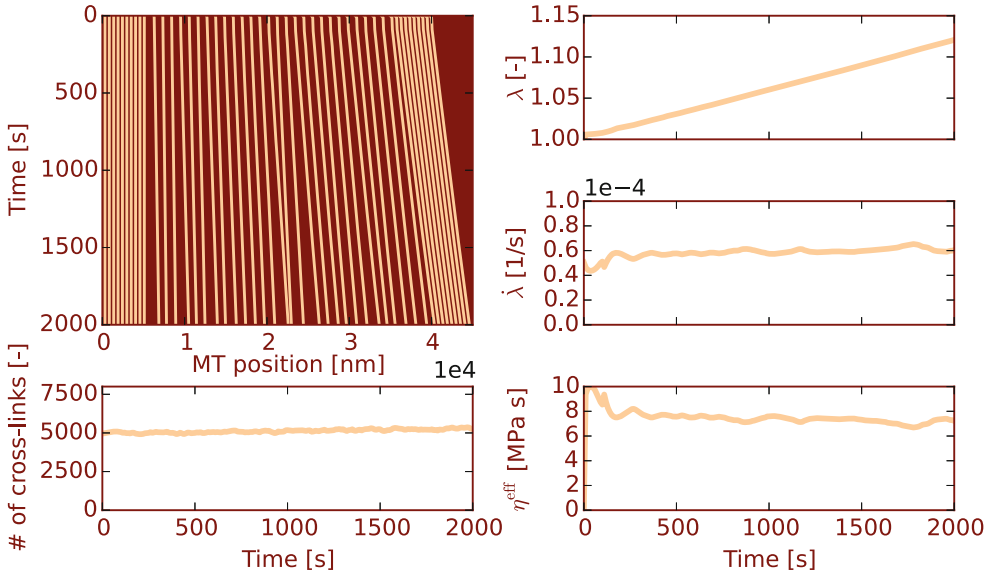

Fig. 9 Axon with dissipative dynamic mechanism assigned to each crosslink and loaded by an external tip force. The typical readout of a single simulation includes a kymograph (*top left*), the total number of crosslinks vs time (*bottom left*), axon stretch vs time (*top right*), axon stretch rate vs time (*middle right*), and axon viscosity vs time (*bottom right*)

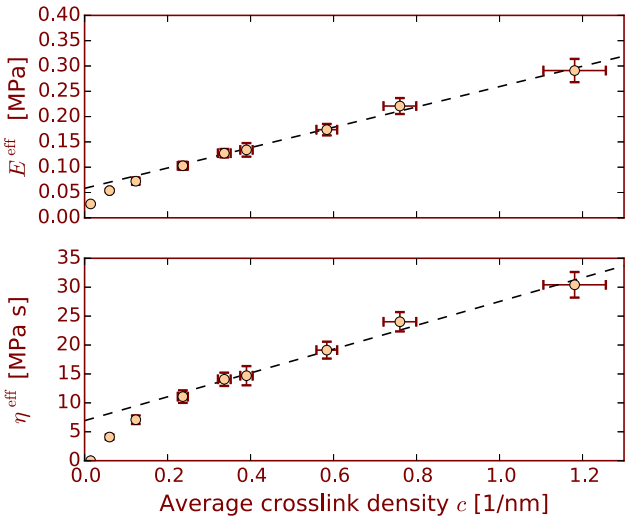

Fig. 10 Axon stiffness E^{eff} and axon viscosity η^{eff} as emergent properties in terms of the average crosslink density c. *Data points* and *error bars* indicate the means and standard deviations. For crosslink densities above $0.2\,\text{nm}^{-1}$, both stiffness and viscosity increase linearly with increasing crosslink density; for crosslink densities below $0.2\,\text{nm}^{-1}$, stiffness and viscosity decrease rapidly to zero

two most relevant parameters, the crosslink density, c, and the characteristic time constant, $\tilde{\tau} = \texttt{tAttach} = \texttt{tDetach}$.

Figure 10 shows the axon stiffness $E = \sigma^{\text{ext}}/\varepsilon$ and the axon viscosity $\eta = \sigma^{\text{ext}}/\dot{\varepsilon}$ as functions of the crosslink density c calculated as the number of crosslinks per axon unit length. The data points represents the mean stiffnesses and viscosities of n = 15 simulations; the error bars represent the standard deviations generated by the randomness in our model. Since the average crosslink density is only controlled indirectly by the longitudinal distance between two consecutive crosslinks, it is also a random variable with corresponding means and standard deviations. Both axon stiffness and viscosity increase linearly with the density of crosslinks for an axon density above $0.2\,\text{nm}^{-1}$. For smaller crosslink densities, the stiffness and viscosity rapidly decrease to zero. Both observations are consistent with a previous report [41]: The rapid decrease of stiffness and viscosity at low crosslink densities is a natural result of the reduction of available load paths within the axon as described by the percolation theory. Indeed, microtubules that would be connected at high crosslinks densities become disconnected when less crosslinks are available.

Figure 11 shows the effective axon stiffness $E^{\text{eff}} = E/[1+c_\tau\,\Delta t/\tilde{\tau}]$, the axon viscosity $\eta = \tilde{\tau}\,E/c_\tau$, the effective relaxation time $\tau^{\text{eff}} = \eta/E^{\text{eff}}$, and the normalized detachment and reattachment time $\tilde{\tau}/\tau^{\text{eff}} = c_\tau/[1 + c_\tau\,\Delta t/\tilde{\tau}]$ as functions of the characteristic detachment and reattachment time $\tilde{\tau}$. Here we have reparameterized the relaxation time $\tau = \tilde{\tau}/c_\tau$ via the characteristic detachment and reattachment time $\tilde{\tau}$ scaled by the rate constant $1/c_\tau$. The data points represents the mean values of n = 15 simulations; the error bars represent the standard deviations generated by the randomness in our model. The dashed lines represent the best fit to the viscoelastic Maxwell model as described by the equations above. The two curves in each plot are generated by the same data, but with different axon stiffnesses using $\Delta t = 0\,\text{s}$, shown in blue, and $\Delta t = 100\,\text{s}$, shown in orange.

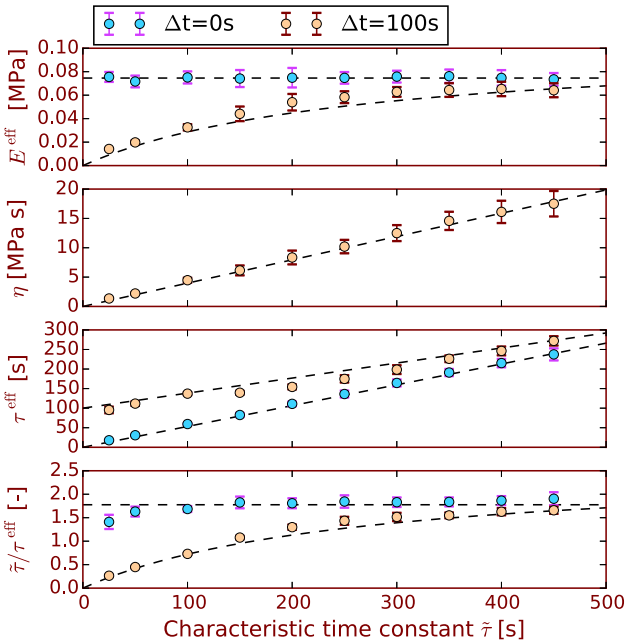

Fig. 11 Effective axon stiffness E^{eff} and axon viscosity η as emergent properties in terms of the characteristic detachment and reattachment time $\tilde{\tau}$. *Data points* and *error bars* indicate the means and standard deviations. *Dashed lines* represent the best fit to the viscoelastic Maxwell model

The only difference between these curves is that we measured stiffness as the ratio of stress and strain after the 1st and 11th time step for $\Delta t = 0\,\text{s}$ and $\Delta t = 100\,\text{s}$ respectively. We performed individual fits for $\Delta t = 0\,\text{s}$ and $\Delta t = 100\,\text{s}$, and obtained different values for E and c_τ for the two curves. The numerical simulations nicely agree with the analytical predictions.

5.2 Active motor crosslinking

To explore the effects of the molecular mechanism of active motor crosslinking on whole axon rheology, we use the axon model from Sect. 3 and assign the dynein motor mechanism of Sect. 4.2 to all crosslinks. On the molecular level, the crosslinks detach, elongate to reattach, and actively contract during the dynein power stroke as they return to their initial length. On the axon level, this behavior collectively generates internal stresses in the axon.

Figure 12 highlights the three different scenarios that can occur on the axon level in response to different dynein configurations: extension, neutral deformation, and contraction. Dynein is a molecular motor that walks towards the minus end of the microtubule. If the fixed domain of each dynein crosslink is located closer to the plus end of the microtubule, the powerstroke of dynein induces axonal elongation. If the fixed domain is located closer to the minus end, the powerstroke induces axonal contraction. The tendencies towards

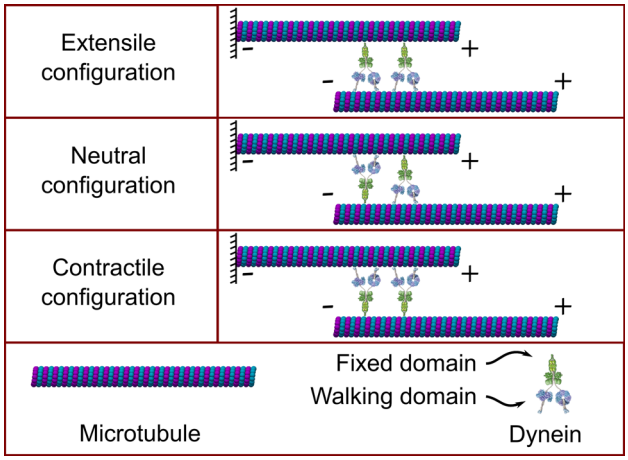

Fig. 12 Different dynein configurations and their effects on internal force generation within the axon. When the fixed domains of the dynein motors are predominantly located at the plus ends of the microtubulues, the configuration extends (*top*); when the fixed domains are located at the minus ends, the configuration contracts (*bottom*); when the fixed domains are evenly distributed, the configuration remains neutral (*middle*)

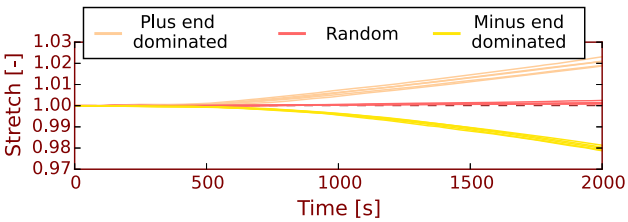

Fig. 13 Axon with dynein motor mechanism assigned to each crosslink. Axonal stretch λ as a function of time t for $n=15$ simulations. For $n=5$ simulations with the fixed domains of the dynein motors predominantly located at the plus ends of the microtubulues, the axonal stretch is extensile (*orange*); for $n=5$ simulations with the fixed domains located at the minus ends, the axonal stretch is contractile (*yellow*); for $n=5$ simulations with random orientation, the axonal stretch remains neutral (*red*). (Color figure online)

elongation and contraction cancel out if all fixed domains are randomly oriented.

Figure 13 illustrates a simulation of the three different scenarios, extensile, contractile, and neutral, for a total of $n=15$ simulations of which $n=5$ have the fixed domains of the dynein motors predominantly located at the plus ends of the microtubulues, $n=5$ have the fixed domains located at the minus ends, and $n=5$ have a random orientations. We clearly observe the expected difference in axon behavior for the three different configurations of the dynein crosslinks: The axonal stretch is extensile for the fixed domains located near the plus ends, contractile for the fixed domains located near the minus ends, and neutral for random orientations. Recent experiments have shown that the fixed domains of dynein are predominantly associated with the plus end of microtubules [63,75] and that dynein plays a critical role

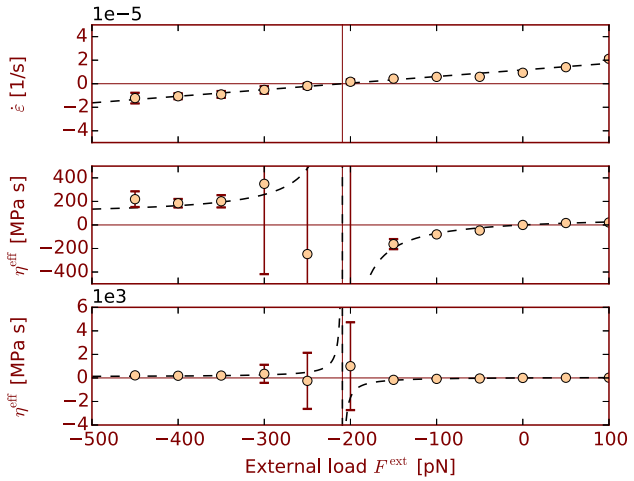

Fig. 14 Axon stretch rate $\dot{\varepsilon}$ (*top*) and effective axon viscosity η^{eff} (*middle* and *bottom*) as a function of the external force with the fixed domains of all dynein motors located at the plus ends of the microtubulues to generate axonal extension. *Data points* and *error bars* indicate the means and standard deviations; numbers below each data point indicate the number of simulations used to create the data point. *Dashed lines* represent the best fit to the viscoelastic Maxwell model with internal force generation. The internal force that emerges from active motor crosslinking, $F^{\text{int}} = 210\,\text{pN}$, is the negative of the external force at a mean stretch rate of zero, $F^{\text{ext}} = -210\,\text{pN}$ (*top*)

in axonal elongation [9,65]. These experiments suggest the extensile configuration in Fig. 12 is the most physiologically relevant. In turn the modeling in Fig. 13 suggests the experimentally observed pushing force generated by dynein [65] arises as direct consequence the molecular association of the dynein cargo binding domain with microtubule plus tip proteins.

Figure 14 shows the stretch rate $\dot{\varepsilon} = [\,\sigma^{\text{ext}} + \sigma^{\text{int}}\,]/\eta = [\,F^{\text{ext}} + F^{\text{int}}\,]/[\,\eta A^{\text{axn}}\,]$ and effective viscosity $\eta^{\text{eff}} = \eta/[\,1 + \sigma^{\text{int}}/\sigma^{\text{ext}}\,] = \eta/[\,1 + F^{\text{int}}/F^{\text{ext}}\,]$ plotted versus the external force F^{ext}. For these simulations, we use the same model as before, now with all dynein motors located at the plus ends of the microtubulues to generate a net internal force F^{int}, which we balance by an external tip force F^{ext} that we vary from -500 to 100 pN. The values for the internal force F^{int} and the viscosity η are unknown a priori, both emerge as axon-level properties of our axon model. Figure 14, top, provides the external force at a mean stretch rate of zero, $F^{\text{ext}} = -210\,\text{pN}$, which, by force equilibrium, $F^{\text{ext}} + F^{\text{int}} = 0\,\text{pN}$, defines the internal force that emerges from active motor crosslinking, $F^{\text{int}} = -F^{\text{ext}} = 210\,\text{pN}$. We can then calculate the viscosity $\eta^{\text{eff}} = \dot{\varepsilon}\,A^{\text{axn}}/[\,F^{\text{ext}} + F^{\text{int}}\,]$, which approaches infinity $\eta^{\text{eff}} \to \pm\infty$ for $F^{\text{int}} \to -F^{\text{ext}}$. Naturally, the numerical predictions for viscosity are not able to capture this region accurately as a slight deviations in the computed stretch rate lead to enormous variations in the computed effective viscosity. However, our model captures the analytical predictions well for $\left|F^{\text{ext}} - F^{\text{int}}\right| > 100\,\text{pN}$.

6 Discussion

Molecular mechanisms play a critical role in modulating axonal physiology, both by transmitting passive forces and by generating active forces. Here we created a generic axon model to simulate molecular mechanisms within the context of the finite element method. Our infrastructure preserves the inherent modularity of the finite element method and, at the same time, allows us integrate in a wide range of molecular mechanisms (Fig. 2). To illustrate the fundamental features of our approach, we created an axon model of discrete microtubules that are aligned along the axon and connected to neighboring microtubules by discrete crosslinking mechanisms (Figs. 3, 4). Our axon model naturally connects molecular-level events to axon-level properties and allows us to explore how characteristic axonal features emerge from the collective interaction of individual molecular mechanisms. What makes our finite element model unique is that a fluid-like behavior (Figs. 10, 11) arises solely from a collection of springs, which dynamically make and break connections by a set of simple rules (Figs. 6, 7). The different configurations of our model naturally capture the idea fundamental to active matter hydrodynamics that the relative orientation of internal and external force vectors profoundly influences the effective viscoelastic properties of soft matter (Figs. 12, 13). We highlight these features by means of two examples: passive dissipative crosslinking and active motor crosslinking. By assigning different mechanisms to standard finite elements, we automatically embed these molecular-level events within the solution procedure throughout the entire simulation.

Passive dissipative crosslinking characterizes a passive detachment and reattachment of a crosslink from and to the microtubule. A key feature of passive dissipative crosslinking is that each crosslink detaches at the elongated state and reattaches at its original rest length, which generates energy dissipation and, on the axon level, an emergent rheology that is conceptually similar to viscosity [15,22]. The major molecular-level parameters that govern these events are the average crosslink density and the characteristic detachment and reattachment time; the main axon-level parameters that emerge from these events are the stiffness and the viscosity. To qualitatively compare our axon simulations to experiments, we extracted kymographs from our simulation and compared them to kymographs of axonal stretch experiments [54,55] (Fig. 8). Simulation and experiment showed a good qualitative agreement. To quantitatively compare molecular-level events to axon-level properties, we performed a series of simulations with systematically varying crosslink densities and detachment and reattachment times. Our simulations reveal that the axon stiffness and viscosity scale linearly with the average crosslink density. The axon as a whole behaves like a viscoelastic Maxwell element [22]: The axon stiffness is independent of the characteristic time constant of the

crosslinks and the viscosity scales linearly with this time constant. The strong non-linear stress strain relationships predicted by active matter hydrodynamics arise elegantly as emergent properties from a system of springs that obey simple rules (Figs. 6, 7). In particular, by allowing springs to make and break connections viscosity arises as an emergent property (Fig. 9). This is consistent with experimental work that has demonstrated that neurons behave are solids or fluids depending on the time scale [10,24,54]. In turn, the time-dependent apparent elasticity and viscosity follow the predictions outlined by the Maxwell fluid equations (Fig. 11), which may be important for developing a better understanding of the complex frequency dependence of neuronal rheological parameters in various experimental regimes [19].

Active motor crosslinking characterizes an active detachment and reattachment of a crosslink from and to the microtubule. A key feature of active motor crosslinking is that each crosslinks detaches at the contracted state and reattaches at its initial length, which generates active contraction and, on the axon level, an emergent rheology that is conceptually similar to an active force or internal stress [6,10,55]. The major molecular-level parameters that govern these events are the average crosslink density and the characteristic detachment and reattachment time; the main axon-level parameters that emerge from these events are the stiffness and the viscosity. Another critical molecular-level parameter that governs these events is the configuration of dynein with respect to the plus and minus ends of the microtubules. Our simulations reveal that the axon extends when the fixed domains of the dynein motors are predominantly located at the plus ends of the microtubulues, it contracts when the fixed domains are located at the minus ends, and it remains neutral when the fixed domains are evenly distributed. In the extensile configuration, the axon as a whole behaves like a viscoelastic Maxwell element with internal stress generation. Importantly, when assessing the effective viscoelastic properties in our active system, effective viscosity has the same non-linear pattern predicted by active matter hydrodynamics [51,56] (Fig. 14). While this is an obvious consequence of the kinematic equations, balance equations, and constitutive equations that govern the system, the model inherently captures the complicated behavior that arises as an emergent property of a few easily understood rules [45,51,59]. This is in line with several recent micro-to-macro approaches proposed in the context of population dynamics [82].

In conclusion, we have created a conceptually novel approach to characterize axon-level parameters as evolving properties from molecular-level events. We have shown that axon elasticity and axon viscosity increase linearly with the crosslink density of microtubules, and that they are highly sensitive to the characteristic crosslink detachment and reattachment times. We have illustrated these effects for both passive and active crosslinking mechanisms. Our simulations explain how dynein, a molecular motor whose fixed domains are predominately associated with the plus end of microtubules, generates internal stresses and drives axon elongation. We anticipate that our model will allow us us probe a wide variety of molecular phenomena—both in isolation and in interaction—to explore their role in modulating characteristic cellular features including stiffness, viscosity, and internal stress.

Acknowledgements This study was supported by the Stanford Graduate Fellowship to Rijk de Rooij and by the Bio-X IIP seed Grant 'Molecular Mechanisms of Chronic Traumatic Encephalopathy' to Ellen Kuhl.

References

1. Abe I, Tsujino A, Hara Y, Ichimura H, Ochiai N (2002) Paranodal demyelination by gradual nerve stretch can be repaired by elongation of internodes. Acta Neuropathol 104:505–512
2. Ahmad FJ, Echeverri CJ, Vallee RB, Baas PW (1998) Cytoplasmic dynein and dynactin are required for the transport of microtubules into the axon. J Cell Biol 140:391–401
3. Ahmad FJ, Hughey J, Wittmann T, Hyman A, Greaser M, Baas PW (2000) Motor proteins regulate force interactions between microtubules and microfilaments in the axon. Nature Cell Biol 2:276–280
4. Ahmadzadeh H, Smith DH, Shenoy VB (2014) Viscoelasticity of tau proteins leads to strain rate-dependent breaking of microtubules during axonal stretch injury: predictions from a mathematical model. Biophys J 106:1123–1133
5. Ahmadzadeh H, Smith DH, Shenoy VB (2015) Mechanical effects of dynamic binding between tau proteins on microtubules during axonal injury. Biophys J 109:2328–2337
6. Ahmed WW, Rajagopalan J, Tofangchi A, Saif TA (2012) Neuromechanics: the role of tension in neuronal growth and memory. Fundamentals and frontiers. Wiley, Chichester
7. Athamneh AIM, Suter DM (2015) Quantifying mechanical force in axonal growth and guidance. Front Cell Neurosci 9:359
8. Ayali A (2010) The function of mechanical tension in neuronal and network development. Integr Biol 2:178–182
9. Baas P (2001) Force generation by cytoskeletal motor proteins as a regulator of axonal elongation and retraction. Trends Cell Biol 11:244–249
10. Bernal R, Pullarkat PA, Melo F (2007) Mechanical properties of axons. Phys Rev Lett 99:018301
11. Betz T, Koch D, Lu YB, Franze K, Käs JA (2011) Growth cones as soft and weak force generators. Proc Natl Acad Sci USA 108:13420–13425
12. Bray D (1979) Mechanical tension produced by nerve cells in tissue culture. J Cell Sci 37:391–410
13. Bray D, Bunge MB (1981) Serial analysis of microtubules in cultured rat sensory axons. J Neurocytol 10:589–605
14. Bridgman PC, Dave S, Asnes CF, Tullio AN, Adelstein RS (2001) Myosin IIB is required for growth cone motility. J Neurosci 21:6159–6169
15. Budday S, Nay R, de Rooij R, Steinmann P, Wyrobek T, Ovaert TC, Kuhl E (2015) Mechanical properties of gray and white matter brain tissue by indentation. J Mech Behav Biomed Mater 46:318–330
16. Burgess SA, Walker ML, Sakakibara H, Knight PJ, Oiwa K (2003) Dynein structure and power stroke. Nature 421:715–718

17. Caminiti R, Carducci F, Piervincenzi C, Battaglia-Mayer A, Confalone G, Visco-Comandini F, Pantano P, Innocenti GM (2013) Diameter, length, speed, and conduction delay of callosal axons in macaque monkeys and humans: comparing data from histology and magnetic resonance imaging diffusion tractography. J Neurosci 33:14501–14511
18. Carter NJ, Cross RA (2005) Mechanics of the kinesin step. Nature 435:308–312
19. Chatelin S, Constantinesco A, Willinger R (2010) Fifty years of brain tissue mechanical testing: From in vitro to in vivo investigations. Biorheology 47:255–276
20. Coles CH, Bradke F (2015) Coordinating neuronal actin-microtubule dynamics. Curr Biol 25:R677–R691
21. Conde C, Cáceres A (2009) Microtubule assembly, organization and dynamics in axons and dendrites. Nat Rev Neurosci 10:319–332
22. de Rooij R, Kuhl E (2016) Constitutive modeling of brain tissue: current perspectives. Appl Mech Rev 68:1–16
23. Debanne D, Campanac E, Bialowas A, Carlier E, Alcaraz G (2011) Axon physiology. Physiol Rev 91(2):555–602
24. Dennerll TJ, Lamoureux P, Buxbaum RE, Heidemann SR (1989) The cytomechanics of axonal elongation and retraction. J Cell Biol 109:3073–3083
25. Franze K, Janmey PA, Guck J (2013) Mechanics in neuronal development and repair. Annu Rev Biomed Eng 15:227–251
26. Franze K, Guck J (2010) The biophysics of neuronal growth. Rep Prog Phys 73:094601
27. Ganguly A, Tang Y, Wang L, Ladt K, Loi J, Dargent B, Leterrier C, Roy S (2015) A dynamic formin-dependent deep F-actin network in axons. J Cell Biol 210:401–417
28. Garcia JA, Pena JM, McHugh S, Jerusalem A (2012) A model of the spatially dependent mechanical properties of the axon during its growth. Comput Model Eng Sci 87:411–432
29. Garcia-Grajales JA, Jerusalem A, Goriely A (2016) Continuum mechanical modeling of axonal growth. Comput Methods Appl Mech Eng. doi:10.1016/j.cma.2016.07.032
30. Gennerich A, Carter AP, Reck-Peterson SL, Vale RD (2007) Force-induced bidirectional stepping of cytoplasmic dynein. Cell 131:952–965
31. Gittes F, Mickey B, Nettleton J, Howard J (1993) Flexural rigidity of microtubules and actin filaments measured from thermal fluctuations in shape. J Cell Biol 120:923–934
32. Göktepe S, Menzel A, Kuhl E (2014) The generalized Hill model: a kinematic approach towards active muscle contraction. J Mech Phys Solids 72:20–39
33. Goldberg JL (2003) How does an axon grow? Genes Dev 17:941–958
34. Goriely A, Budday S, Kuhl E (2015) Neuromechanics: from neurons to brain. Adv Appl Mech 48:79–139
35. Goriely A, Geers MGD, Holzapfel GA, Jayamohan J, Jérusalem A, Sivaloganathan S, Squier W, van Dommelen JAW, Waters S, Kuhl E (2015) Mechanics of the brain: perspectives, challenges, and opportunities. Biomech Model Mechanobiol 14:931–965
36. Hällström W, Lexholm M, Suyatin DB, Hammarin G, Hessman D, Samuelson L, Montelius L, Kanje M, Prinz CN (2010) Fifteen-piconewton force detection from neural growth cones using nanowire arrays. Nano Lett 10:782–787
37. Hill AV (1938) The heat of shortening and the dynamic constants of muscle. Proc R Soc B 126:136–195
38. Hirokawa N (1982) Cross-linker system between neurofilaments, microtubules and membranous organelles in frog axons revealed by the quick-freeze, deep-etching method. J Cell Biol 94:129–142
39. Holland MA, Miller KE, Kuhl E (2015) Emerging brain morphologies from axonal elongation. Ann Biomed Eng 43:1640–1653
40. Hyland C, Mertz AF, Forscher P, Dufresne E (2014) Dynamic peripheral traction forces balance stable neurite tension in regenerating Aplysia bag cell neurons. Sci Rep 4:4961
41. Jakobs M, Franze K, Zemel A (2015) Force generation by molecular-motor-powered microtubule bundles; implications for neuronal polarization and growth. Front Cell Neurosci 9:2761
42. Kawamura Y, Dyck PJ, Shimono M, Okazaki H, Tateishi J, Doi H (1981) Morphometric comparison of the vulnerability of peripheral motor and sensory neurons in amyotrophic lateral sclerosis. J Neuropathol Exp Neurol 40:667–675
43. King SM (2011) Dyneins: structure, biology and disease. Academic Press, Boston
44. Koch D, Rosoff WJ, Jiang J, Geller HM, Urbach JS (2012) Strength in the periphery: growth cone biomechanics and substrate rigidity response in peripheral and central nervous system neurons. Biophys J 102:452–460
45. Kollmannsberger P, Fabry B (2011) Linear and nonlinear rheology of living cells. Annu Rev Mater Res 41:75–97
46. Lamoureux P, Buxbaum RE, Heidemann SR (1989) Direct evidence that growth cones pull. Nature 340:159–162
47. Lamoureux P, Heidemann SR, Martzke NR, Miller KE (2010) Growth and elongation within and along the axon. Dev Neurobiol 70:135–149
48. Lowery LA, Vactor DV (2009) The trip of the tip: understanding the growth cone machinery. Nat Rev Mol Cell Biol 10:332–343
49. Lu W, Fox P, Lakonishok M, Davidson MW, Gelfand VI (2013) Initial neurite outgrowth in drosophila neurons is driven by kinesin-powered microtubule sliding. Curr Biol 23:1018–1023
50. Mallik R, Carter BC, Lex SA, King SJ, Gross SP (2004) Cytoplasmic dynein functions as a gear in response to load. Nature 427:649–652
51. Marchetti MC, Joanny JF, Ramaswamy S, Liverpool TB, Prost J, Rao M, Simha RA (2013) Hydrodynamics of soft active matter. Rev Model Phys 85:1143–1189
52. Moulton DE, Lessinnes T, Goriely A (2013) Morphoelastic rods. Part I: a single growing elastic rod. J Mech Phys Solids 61:398–427
53. Nagy S, Ricca BL, Norstrom MF, Courson DS, Brawley CM, Smithback PA, Rock RS (2008) A myosin motor that selects bundled actin for motility. Proc Natl Acad Sci USA 105:9616–9620
54. O'Toole M, Lamoureux P, Miller KE (2008) A physical model of axonal elongation: force, viscosity, and adhesions govern the mode of outgrowth. Biophys J 94:2610–2620
55. O'Toole M, Lamoureux P, Miller KE (2015) Measurement of subcellular force generation in neurons. Biophys J 108:1027–1037
56. O'Toole M, Lamoureux P, Miller KE (2016) Forces control effective viscosity in neurons (submitted for publication)
57. Pannese E (2015) Neurocytology: fine structure of neurons, nerve processes, and neuroglial cells. Springer, Berlin
58. Peter SJ, Mofrad MRK (2012) Computational modeling of axonal microtubule bundles under tension. Biophys J 102:749–757
59. Pritchard RH, Huang YYS, Terentjev EM (2014) Mechanics of biological networks: from the cell cytoskeleton to connective tissue. Soft Matter 10:1864–1884
60. Rajagopalan J, Tofangchi A, Saif T (2010) Drosophila neurons actively regulate axonal tension in vivo. Biophys J 99:3208–3215
61. Rausch MK, Kuhl E (2013) On the effect of prestrain and residual stress in thin biological membranes. J Mech Phys Solids 61:1955–1969
62. Recho P, Jérusalem A, Goriely A (2016) Growth, collapse, and stalling in a mechanical model for neurite motility. Phys Rev E 93:032410
63. Roberts AJ, Goodman BS, Reck-Peterson SL, Balasubramanian M (2014) Reconstitution of dynein transport to the microtubule plus end by kinesin. eLife 3:e02641

64. Rodriguez ML, McGarry PJ, Sniadecki NJ (2013) Review on cell mechanics: experimental and modeling approaches. Appl Mech Rev 65:060801
65. Roossien DH, Lamoureux P, Miller KE (2014) Cytoplasmic dynein pushes the cytoskeletal meshwork forward during axonal elongation. J Cell Sci 127:3593–3602
66. Roossien D, Miller K, Gallo G (2015) Ciliobrevins as tools for studying dynein motor function. Front Cell Neurosci 9:252
67. Siechen S, Yang S, Chiba A, Saif T (2009) Mechanical tension contributes to clustering of neurotransmitter vesicles at presynaptic terminals. Proc Natl Acad Sci USA 106:12611–12616
68. Smith DH (2009) Stretch growth of integrated axon tracts: extremes and exploitations. Prog Neurobiol 89:231–239
69. Soheilypour M, Peyro M, Peter SJ, Mofrad MRK (2015) Buckling behavior of individual and bundled microtubules. Biophys J 108:1718–1726
70. Suresh S (2006) Biomechanics and biophysics of cancer cells. Acta Biomater 3:413–438
71. Suter DM, Miller KE (2011) The emerging role of forces in axonal elongation. Prog Neurobiol 94:91–101
72. Toba S, Watanabe TM, Yamaguchi-Okimoto L, Toyoshima YY, Higuchi H (2006) Overlapping hand-over-hand mechanism of single molecular motility of cytoplasmic dynein. Proc Natl Acad Sci USA 103:5741–5745
73. Vale RD (2003) The molecular motor toolbox for intracellular transport. Cell 112:467–480
74. van den Bedem H, Kuhl E (2015) Tau-ism: the yin and yang of microtubule sliding, detachment, and rupture. Biophys J 109:2215–2217
75. Vaughan KT, Tynan SH, Faulkner NE, Echeverri CJ, Vallee RB (1999) Colocalization of cytoplasmic dynein with dynactin and CLIP-170 at microtubule distal ends. J Cell Sci 112:1437–1447
76. Xu K, Zhong G, Zhuang X (2013) Actin, spectrin, and associated proteins form a periodic cytoskeletal structure in axons. Science 339:452–456
77. Yildiz A, Selvin P (2005) Kinesin: walking, crawling or sliding along? Trends Cell Biol 15:112–120
78. Yu W, Baas PW (1994) Changes in microtubule number and length during axon differentiation. J Neurosci 14:2818–2829
79. Zemel A, Mogilner A (2009) Motor-induced sliding of microtubule and actin bundles. Phys Chem Chem Phys 11:4821–4833
80. Zhang H, Berg JS, Li Z, Wang Y, Lång P, Sousa AD, Bhaskar A, Cheney RE, Strömblad S (2004) Myosin-X provides a motor-based link between integrins and the cytoskeleton. Nat Cell Bio 6:523–531
81. Zohdi TI (2007) A computational framework for network modeling of fibrous biological tissue deformation and rupture. Comput Methods Appl Mech Eng 196:2972–2980
82. Zohdi TI (2016) An agent-based computational framework for simulation of competing hostile planet-wide populations. Comput Methods Appl Mech Eng. doi:10.1016/j.cma.2016.04.032
83. Zöllner AM, Abilez OJ, Böl M, Kuhl E (2012) Stretching skeletal muscle: chronic muscle lengthening through sarcomerogenesis. PLoS ONE 7:e45661